International Journal of Hyperthermia

ISSN: 0265-6736 (Print) 1464-5157 (Online) Journal homepage: informahealthcare.com/journals/ihyt20

Optimization of the sources in local hyperthermia using a combined finite element-genetic algorithm method

N. Siauve, L. Nicolas, C. Vollaire & C. Marchal

To cite this article: N. Siauve, L. Nicolas, C. Vollaire & C. Marchal (2004) Optimization of the sources in local hyperthermia using a combined finite element-genetic algorithm method, International Journal of Hyperthermia, 20:8, 815-833, DOI: 10.1080/02656730410001711664

To link to this article: https://doi.org/10.1080/02656730410001711664

INT. J. HYPERTHERMIA
VOL. 20, NO. 8 (DECEMBER 2004), pp. 815–833

Taylor & Francis
healthsciences

Optimization of the sources in local hyperthermia using a combined finite element-genetic algorithm method

N. SIAUVE†*, L. NICOLAS‡, C. VOLLAIRE‡ and C. MARCHAL§

† CEGELY, UMR CNRS 5005, Université C. Bernard Lyon 1,
69622 Villeurbanne Cedex, France
‡ CEGELY, UMR CNRS 5005, Ecole Centrale de Lyon, 69134 Ecully Cedex,
France
§ Unité d'hyperthermie, Centre Alexis Vautrin, 54551 Vandœuvre-lès-Nancy,
France

(*Received 29 September 2003; revised 9 February 2004; accepted 12 April 2004*)

This article describes an optimization process specially designed for local and regional hyperthermia in order to achieve the desired specific absorption rate in the patient. It is based on a genetic algorithm coupled to a finite element formulation. The optimization method is applied to real human organs meshes assembled from computerized tomography scans. A 3D finite element formulation is used to calculate the electromagnetic field in the patient, achieved by radiofrequency or microwave sources. Space discretization is performed using incomplete first order edge elements. The sparse complex symmetric matrix equation is solved using a conjugate gradient solver with potential projection pre-conditionning. The formulation is validated by comparison of calculated specific absorption rate distributions in a phantom to temperature measurements. A genetic algorithm is used to optimize the specific absorption rate distribution to predict the phases and amplitudes of the sources leading to the best focalization. The objective function is defined as the specific absorption rate ratio in the tumour and healthy tissues. Several constraints, regarding the specific absorption rate in tumour and the total power in the patient, may be prescribed. Results obtained with two types of applicators (waveguides and annular phased array) are presented and show the faculties of the developed optimization process.

Key words: Electromagnetic heating, finite element method, genetic algorithm, hyperthermia treatment planning, specific absorption rate, optimization

1. Introduction

Hyperthermia as a method of treating cancer has a long history. The treatment of cancer with hyperthermia can be traced back to 3000 BC when smoldering sticks of wood were inserted in tumours. In 1893, Coley[1] used bacterial toxins to raise the temperature in patients which resulted in tumour regression. The strategy of modern anti-cancer therapy is directed towards local control of tumour growth with maximal possible elimination of the neoplastic cell load. Many clinical studies have established that elevated cancer cell temperature enhances the effect of chemotherapy and radiation therapy in the treatment of tumours in the human body[2–5].

This local elevation of temperature in the tumour can be realized principally with ultrasound waves[6,7] or electromagnetic (EM) fields. The present work is dedicated to hyperthermia with electromagnetic fields. Hyperthermia with radiofrequency[8] (RF) or microwave[9] radiating devices is administered in several treatment sessions. With this therapy, the malignant tumour is heated at temperatures between 42–44°C

* To whom correspondence should be addressed. e-mail: siauve@cegely.univ-lyon1.fr

International Journal of Hyperthermia ISSN 0265–6736 print/ISSN 1464–5157 online
http://www.tandf.co.uk/journals
DOI: 10.1080/02656730410001711664

for 30–60 min[10]. During treatment with RF or microwave devices, the physicians have had difficulty adequately heating tumours while preserving surrounding healthy tissues. Furthermore, clinical studies in hyperthermia have shown the difficulty to measure the temperature distribution in the patient during the hyperthermia sessions[11]. The study presented in this article involves a Finite Element (FE)–Genetic Algorithm (GA) method to improve the distribution of electromagnetic energy deposition in the patient during hyperthermia treatment.

Hyperthermia treatment requires the generation of an appropriate temperature distribution in the body of an individual patient. When the heating is induced by radio waves, several antennae are used, each of which can be steered independently in wave amplitude and phase, to achieve favourable interference patterns. The objective of numerical simulations is to provide *a-priori* information for an optimal adjustment of wave amplitude and phase of each antenna to reduce the RF energy absorption in nearby healthy tissues while focusing into the deep-seated tumour. The numerical simulation involves two steps: calculation of the resulting electromagnetic fields inside the inhomogeneous body by solving Maxwell's equations and the optimization of the Specific Absorption Rate (SAR) distribution in the patient during the hyperthermia sessions.

To determine numerically the electric field repartition for hyperthermia problems with electromagnetic wave in the frequency range 1 MHz–2.5 GHz, the principal methods used are the finite difference time domain[12,13] and the finite element[14]. Several other formulations have also been reported such as the method of moments[15] or the volume surface integral equation, but their use seems to be less widespread. For this hyperthermia treatment planning application, the FE technique was chosen to model the SAR repartition. The FE method has shown its capability to handle heterogeneous structures and the utilization of tetrahedral elements and is really appropriate to model with accuracy the curved interface such as those found in human bodies.

Prior to heating tumours, treatment planning based on an accurate prediction of temperature distribution is essential. This prediction of temperature distribution needs the knowledge of the optimal SAR repartition. This paper introduces a novel individual treatment plan to achieve optimal SAR distribution combining FE and GA and shows its possible clinical utilization. The three-dimensional FE method based on edge elements were used for the computation of E-fields and SAR distribution. A simulation tool for the prediction of the EM fields and SAR due to RF or microwave fields was developed. The prediction tool has been validated against temperature measurements performed on a phantom irradiated with a waveguide applicator operating at 27.12 MHz and compared to computed SAR. The segmentation of the patient is realized from computerized tomography (CT) data sets that allow one to take into account the real shape of the patient and the tumour. A flexible local hyperthermia treatment planning has been devised, presented and tested on two configurations including the patient model and the hyperthermia systems: Annular Phased Array (APA) functioning at 110 MHz and waveguides device operating at 27.12 MHz.

2. Methods

The treatment planning tool is based on the FE method to model the SAR distribution and on the genetic algorithm to realize the optimization of the SAR distribution in the patient.

2.1. *Electric field computation*

The dielectric materials as biological tissues have a dielectric constant $\varepsilon_{\text{real}}$ and loss factor $\varepsilon_{\text{imag}}$. The interaction between the **E** field and the biological tissue is described in terms of the complex permittivity,ε:

$$\varepsilon = \varepsilon_c \varepsilon_0 = (\varepsilon_{\text{real}} - j\varepsilon_{\text{imag}})\varepsilon_0 \tag{1}$$

The dielectric constant, $\varepsilon_{\text{real}}$, represents the ability to store electric field energy and the loss factor, $\varepsilon_{\text{imag}}$, describes a part of energy dissipated in the dielectric material. The loss factor $\varepsilon_{\text{imag}}$ is given by:

$$\varepsilon_{\text{imag}} = \frac{\sigma}{\omega\varepsilon_0} \tag{2}$$

where σ is the conductivity (Sm^{-1}), ω the angular frequency (rds^{-1}) and $\varepsilon_0 = 1/36\pi\, 10^9$ (Fm^{-1}).

The interaction between the RF or microwave field applied and the tissues create oscillation of the free charge carriers and the dipole, at the frequency of the applied fields. The consequence is an elevation of the temperature within the material due to the molecular friction. Hyperthermia with EM fields is based on these heating mechanisms to raise the temperature of the tumour volume.

The Maxwell equations that dictate the propagation of the electromagnetic waves are solved by using the finite element method. A tetrahedral mesh is used for the discretization of the solution area to get a faithful representation of complicated tissue boundaries and intricate hyperthermia applicator structures. As the antennae of the applicator are driven with a fixed angular frequency ω, one can solve Maxwell's equations in the frequency domain:

$$\nabla \times \mathbf{H} = j\omega\varepsilon\mathbf{E} + \mathrm{J_e} \tag{3}$$

$$\nabla\mathbf{B} = 0 \tag{4}$$

$$\nabla \times \mathbf{E} = -j\omega\mu_0\mathbf{H} \tag{5}$$

$$\nabla\mathbf{D} = 0 \tag{6}$$

where **E** is the complex electric field, **H** the complex magnetic field, ω the angular frequency, ε, σ and μ the electrical permittivity, the electrical conductivity and the magnetic permeability of the tissues, respectively, ε is a complex quantity defined by equation (1). Both $\varepsilon_{\text{real}}$ and σ depend on frequency, μ being constant and equal to the free space value. The electric current density $\mathbf{J_e}$ (Åm^{-2}) can be obtained from Ohm's law:

$$\mathbf{J_e} = \sigma\mathbf{E}. \tag{7}$$

In dielectric media no free charges and surface currents are present. Then a standard consideration shows that on interfaces between different media 1 and 2 the continuity relations for the electromagnetic field components are:

$$\mathbf{n} \times (\mathbf{E}_1 - \mathbf{E}_2) = 0 \tag{8}$$

$$\mathbf{n} \times (\varepsilon_1\mathbf{E}_1 - \varepsilon_2\mathbf{E}_2) = 0. \tag{9}$$

Since tissue interfaces can influence the electromagnetic field considerably, the tetrahedral element should resolve these boundary contours well.

Additionally, care has to be taken to enforce physically correct continuity relations for the electromagnetic field components in numerical simulations. This requirement is fulfilled by employing edge elements, which are also called Whitney elements[16,17].

The finite element formulation is given by:

$$-\int_v \nabla W \times \nabla \times \mathbf{E}\, dv - \int_v W k_0^2 \varepsilon_c \mathbf{E}\, dv + \int_{s_{ext}} W g_{ABC}(\mathbf{E})\, ds = -j\omega\mu_0 \int_\Gamma W \mathbf{J_e}\, dv \quad (10)$$

with $k_0 = \omega\sqrt{\mu_0\varepsilon_0}$ and W is the weighting function. In order to take into account the wave propagation out of the FE domain, the FE formulation is coupled with a first order vector Engquist Majda Absorbing Boundaries Condition (ABC)[18]:

$$n \times \nabla \times \mathbf{E} \cong g_{ABC}(\mathbf{E}) = jk_0 \mathbf{E_t} \quad (11)$$

with $\mathbf{E_t}$ the tangential electric field.

Numerical discretization of equation (10) allows one to obtain a linear equation system $Ax = b$. A specific difficulty arises in the solution of this equation system. The resulting matrix A is symmetric, sparse and comprises several hundreds of thousands degrees of freedom. An iterative method is used to solve the matrix system, a conjugate gradient solver with a potential projection pre-conditioning technique.

Figure 1 shows the algorithm for the potential projection pre-conditioning for the conjugate gradient solver. The algorithm of the pre-conditioning method is classical for the A matrix and takes into account a second matrix A_ϕ by specifically dealing with the scalar potential component. The connection between first order nodal elements (space N_h) and first incomplete order edge elements (space Q_h) enables one to define a transfer operator P: $N_h \rightarrow Q_h$. The matrix for the scalar potential problem is then assembled by Galerkin product $A_\phi = P^T A P$, where A is the edge elements matrix[19].

A relevant quantity for hyperthermia treatment is not the electric field itself but rather the SAR. The electromagnetic energy absorption rate in tissue referred to

Solve $Ax_n = r_n$, x_ϕ designates the potential part of x_n.

1. $x_n \leftarrow 0, x_\phi \leftarrow 0$
2. k **descents** with Gauss-Seidel algorithm on $A_\phi x_\phi = P^T r_n$
3. $x_n \leftarrow x_n + P x_\phi$
4. **1 descent and ascent** with Gauss-Seidel algorithm on $Ax_n = r_n$
5. $x_\phi \leftarrow 0$
6. k **descents** with Gauss-Seidel algorithm on $A_\phi x_\phi = P^T (r_n - Ax_n)$
7. $x_n \leftarrow x_n + P x_\phi$

Figure 1. One iteration of the potential projection pre-conditioning algorithm, generally $k = 1$ or 2.

the SAR (Specific Absorption Rate) or ARD (Absorbed Rate Density) may be expressed as:

$$SAR = \frac{ARD}{\rho} = \frac{1}{2}\frac{\sigma |E_{\max}|^2}{\rho} \tag{12}$$

where $E_{\max}$ is the electrical field strength (maximum value) within the biological tissue (Vm^{-1}), σ is the conductivity (Sm^{-1}) and ρ is the mass density (kgm^{-3}) of the lossy dielectric tissue. The ARD describes the absorbed power per volume (Wm^{-3}), this quantity is directly related to the absorbed power per mass of tissue, which is described by SAR (Wkg^{-1}).

2.2. *Genetic algorithm strategy*

The aim was to determine the phase and amplitude for each antenna leading to the optimal SAR distribution within the patient during the hyperthermia treatment. In general, multi-applicator systems are preferred to single applicator ones. The advantage of the array applicators resides in the ability to move the focal point[20]. With multi-applicator systems a hyperthermia treatment optimization tool is essential.

A GA has been developed to search the optimal settings of each source. GA methods present some great advantages over classical gradient methods: they are able to locate the global optimum and they do not require the use of derivatives.

GA are stochastic optimization methods based on the mechanics of natural selection and natural genetics[21,22]. They work with a population of individuals, each representing a feasible solution in the search space. A fitness score (namely the Objective Function: OF) measures the adaptation of individuals in their environment. The convergence of the population to a global optimum of the space is obtained by applying sequentially the three genetics operators: selection, crossover and mutation[23] (figure 2).

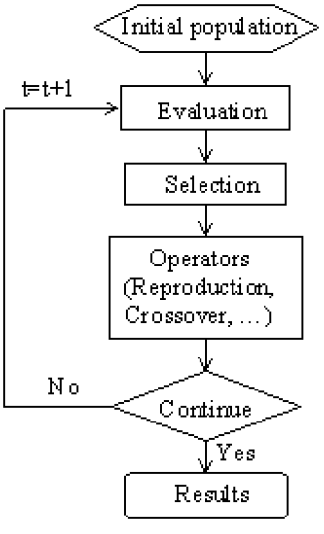

Figure 2. Genetic algorithm procedure.

As the AG proceeds, the selection improves the average fitness of the population while crossovers and mutations explore the solution space. The balance between exploration of the solution space and exploitation of the fittest individuals gives to GA its capability for finding the global optimum.

The implemented GA uses real representation. It is based on random initialization, tournament selection, continue symmetric crossover and local mutation. The population size is fixed to 100 individuals and crossover and mutation probabilities are respectively fixed to 0.5 and 0.01.

The heating is achieved with a set of N antennae surrounding the patient, which are in fixed positions and operate at the same frequency. The free parameters are the phase φ and the amplitude $A_n (n=1,\ldots,N)$ of the emitting antennae. The electric field expression at any point in space is given by:

$$\vec{E}(\vec{r}) = E_x(\vec{r})\exp(j\psi_x(\vec{r}))\vec{e}_x + E_y(\vec{r})\exp(j\psi_y(\vec{r}))\vec{e}_y + E_z(\vec{r})\exp(j\psi_z(\vec{r}))\vec{e}_z \tag{13}$$

where E_x, E_y, E_z, Ψ_x, Ψ_y, Ψ_z represent respectively the modules and the arguments for each components e_x, e_y, e_z of the E-field.

$$\vec{E}(\vec{r}) = \sum_{v}^{x,y,z} E_v(\vec{r})\exp(j\psi_v(\vec{r}))\vec{e}_v \tag{14}$$

$\vec{E}(\vec{r})$ represents the electric field computed when the antenna is driven by a signal of unit amplitude and zero phase. By taking advantage of the linearity of the electric field, the resulting electric field $\vec{E}(A,\varphi;\vec{r})$ at the location r when modifying the amplitude by a factor A and the argument by a diphase φ is obtained by:

$$\vec{E}(A,\varphi;\vec{r}) = A\exp(j\varphi)\sum_{v}^{x,y,z} E_v(\vec{r})\exp(j\psi_v(\vec{r}))\vec{e}_v \tag{15}$$

The total electric field is generated by the superposition of the basic electric fields in equation (15) produced by each individual source, the resulting E-field at any point in space is:

$$\vec{E}(A_1,\ldots,A_n,\varphi_1,\ldots,\varphi_n;\vec{r}) = \sum_{v}^{x,y,z}\sum_{n=1}^{N} A_n E_{v,n}(\vec{r})\exp(j\psi_{v,n}(\vec{r}) + j\varphi_n)\vec{e}_v \tag{16}$$

The SAR distribution was calculated by the following equations:

$$SAR(A_1,\ldots,A_n,\varphi_1,\ldots,\varphi_n;\vec{r}) = \frac{\sigma(\vec{r})}{2\rho(\vec{r})}\left\|\vec{E}(A_1,\ldots,A_n,\varphi_1,\ldots,\varphi_n)\right\|^2 \tag{17}$$

$$SAR(A_1,\ldots,A_n,\varphi_1,\ldots,\varphi_n;\vec{r}) = \frac{\sigma(\vec{r})}{2\rho(\vec{r})}E(A_1,\ldots,A_n,\varphi_1,\ldots,\varphi_n;\vec{r})\times E^*(A_1,\ldots,A_n,\varphi_1,\ldots,\varphi_n;\vec{r}) \tag{18}$$

The fitness function is defined as follows to express the problem in a form of maximization for GA:

$$OF = \frac{\int_{tumour} SAR(r)\,d^3r}{\int_{healthy\ tissues} SAR(r)\,d^3r}. \tag{19}$$

On the other hand, several constraints are prescribed for an optimal treatment: the SAR in the tumour has to be close to $50\,\mathrm{Wkg}^{-1}$ and the power absorbed by the patient has to be lower than 1250 W[24]. To reach therapeutic temperatures of $\sim 42^{\circ}\mathrm{C}$ at least in some parts of such tumours necessitates a power density of ~ 20–$50\,\mathrm{Wkg}^{-1}$ in the target region[25]. The GA allows one to take into account these two constraints.

2.3. *Validation technique*

The accuracy of the FE model is analysed in two ways. First, the model has been validated on an experimental device (phantom). And, in a second step, the model has been used to determine the E-field distribution for a realistic inhomogeneous geometry of a patient stemming from CT scans for example during interstitial hyperthermia treatment.

The E-field model has been validated on a system used in the treatment of deep-seated tumours. The experimental device is made of a phantom and an applicator, which is actually a waveguide (figure 3). The field is generated by an antenna located in the waveguide and operating at 27.12 MHz, the waveguide is filled with water. The phantom is made of a container in plexiglass containing a polyacrilamide gel[26] with electrical properties of human muscle.

Figure 4 shows in detail the phantom geometries and the implantation of the catheters used for the temperature measurement with optical fibre temperature detectors.

The electromagnetic properties of the different media of the experimental measurement device are given in table 1. Therefore, predicted SAR and measured temperature distributions at 10 mm depth and on the symmetry plane in a muscle phantom were compared. The predicted SAR distribution was obtained using the FE model and the measured temperature distribution was obtained using optical fibre

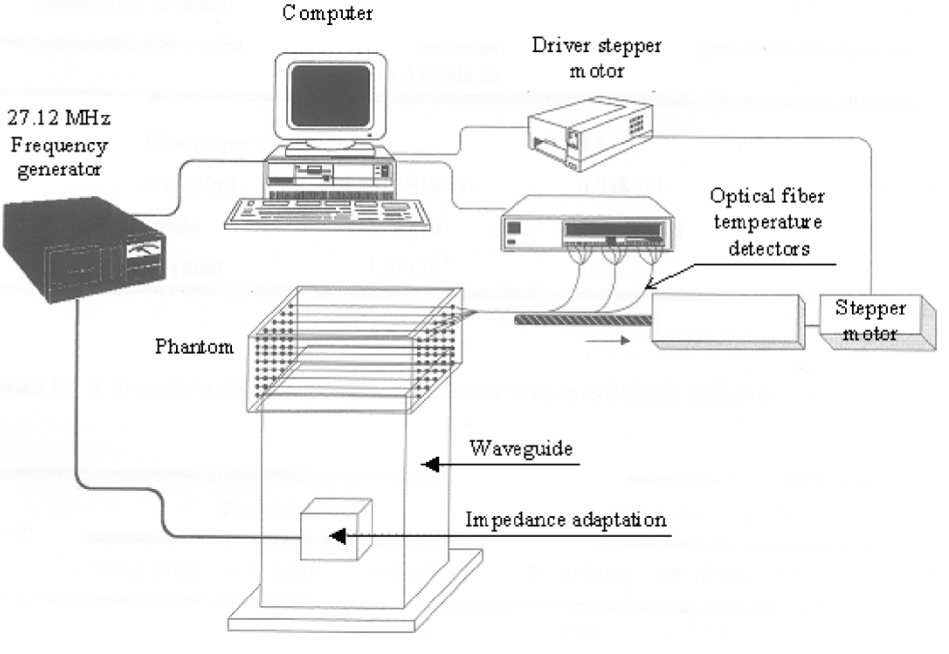

Figure 3. Experimental measurement system[27].

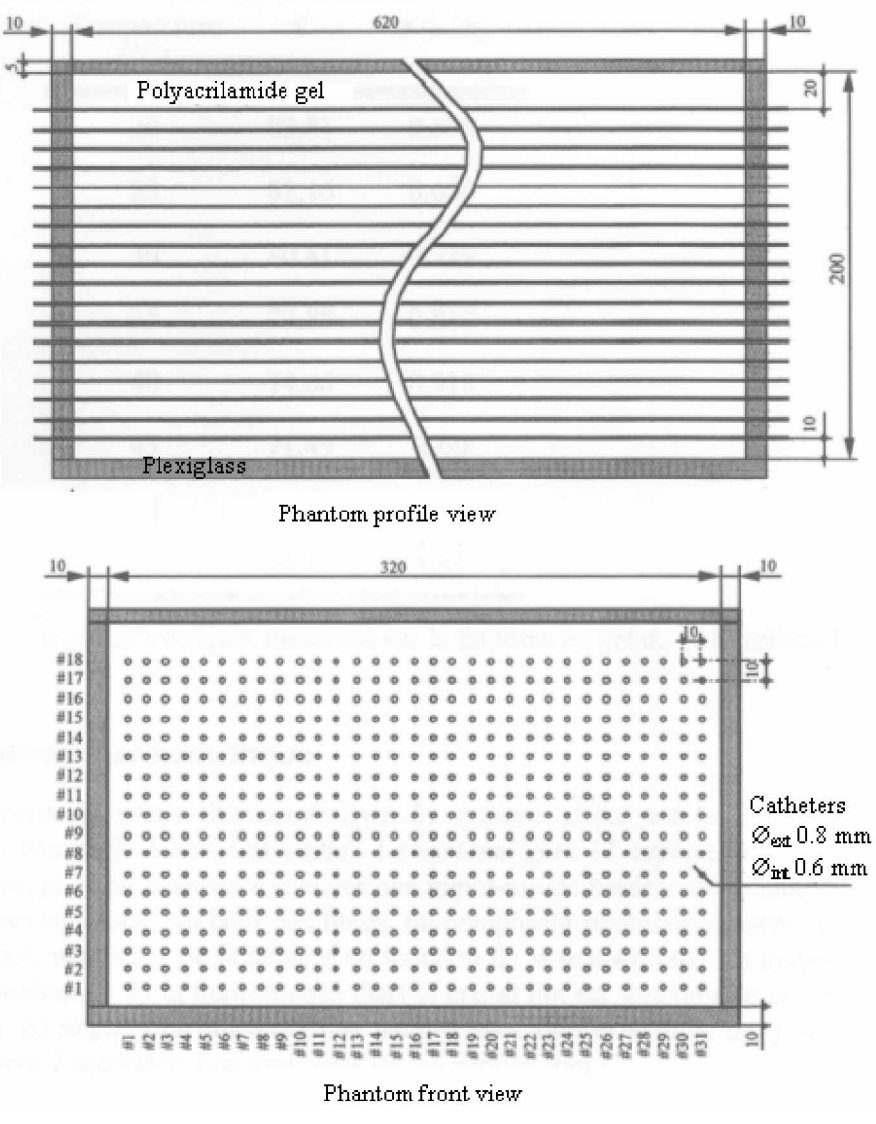

Figure 4. Dimensions of the phantom and implantation of the catheters.

Table 1. Electromagnetic properties of different media at 27.12 MHz.

	Permittivity		Conductivity	Wavelength	Skin depth	Density
	ε_{real}	ε_{imag}	$\sigma\,(\mathrm{Sm}^{-1})$	$\lambda\,(\mathrm{m})$	$\delta\,(\mathrm{m})$	$\rho\,(\mathrm{kgm}^{-3})$
Water	72.5	1.327	0.002	1.3	22.6	1000
Phantom	82.16	431.4	0.65	0.685	0.132	1030
Air	1	0	0	11.06	—	—
Plexiglass	2.5	0	0	7.0	—	1300

temperature detectors. The experimental SAR distribution inside the phantom is obtained by an indirect method. The length of the power pulse is 60 s in order to minimize the effects of the thermal conduction. It has been shown that, is a first approximation, the SAR distribution may be directly related to temperature distribution[28]. If one ignores thermal conduction, the initial temperature rise $\partial T(^\circ C)$ in tissue is related to the SAR:

$$C\frac{\partial T}{\partial t} = SAR \tag{20}$$

where C is the specific heat of the tissue (Joules $\mathrm{kg}^{-1}\,^\circ\mathrm{C}^{-1}$).

2.4. *Segmentation of human patients*

All models presented in this paper are based on three-dimensional CT data sets with a slice distance of 10 mm and a 256×256 resolution. The 10 mm spacing between each CT scans allows one to reconstruct correctly the different organs. It leads to a fit size of the matrix system. A total of at least 60 CT scans including the pelvic region are employed (figure 5). The relevant tissues such as blood, muscle, fat, bone, organs (intestine, liver, bladder, kidneys, spleen) and tumour are defined as homogeneous regions which are manually or semi-automatically segmented with the Amira software[29]. For the segmentation of the patient tetrahedral elements are used. The relative dielectric constant $\varepsilon_{\mathrm{real}}$ and conductivity σ are then assigned to the various regions (tissues and organs), as described in the literature[30–32].

3. Results and discussion

In this section, the different results obtained are presented. First, these results concern the validation of the FE model. Secondly, they concern the results obtained with the optimization procedures on realistic problems.

3.1. *Validation results and discussion*

In a first step, the FE model is validated by comparison of the numerical simulations with the experimental measurements on the device presented in figure 3.

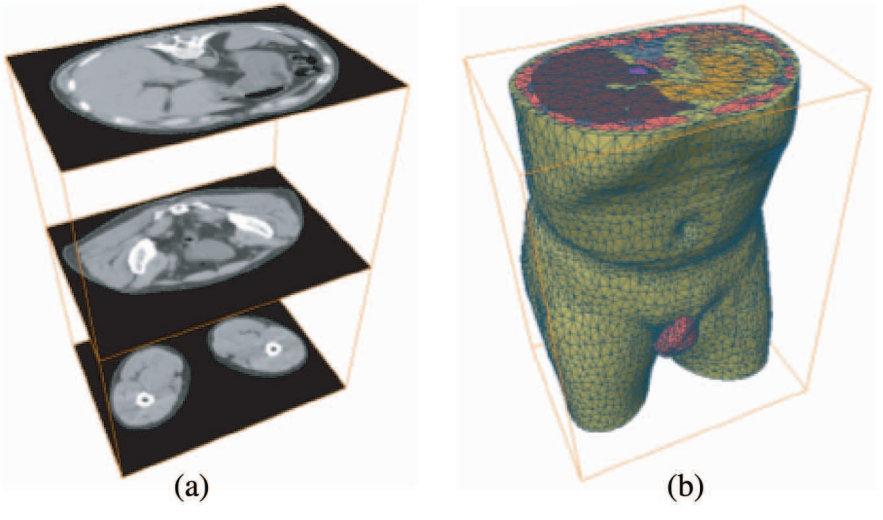

Figure 5. Modelling of the human body (*b*) at the tissues (organs) level from CT scans (*a*).

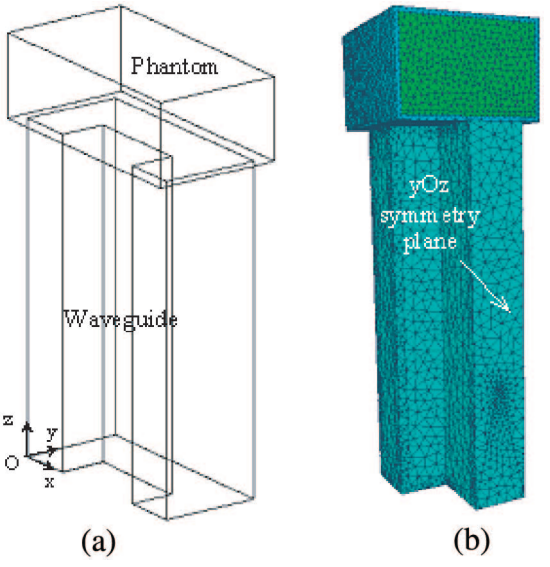

Figure 6. Modelling of the experimental device.

Table 2. Number of iterations and CPU time.

Pre-conditioning	Number of iterations	CPU time* (s)
Cholesky (Gauss algorithm)	12 569	36 389
Cholesky (direct identification)	7 551	25 761
Diagonal	13 561	22 356
SSOR	3 481	12 225
Potential projection	110	3 898

* on HP station J5000 PA risk processor with 1 Go of RAM.

Only half of the experimental hyperthermia system geometry (waveguide and phantom) is described, due to the yOz symmetry plane (figure 6).

Table 2 presents the number of iterations and the CPU time for different pre-conditioning techniques for the conjugate gradient solver in the case of the validation problem shown in figure 6(*b*). The mesh is made of 104 165 tetrahedral elements, 20 337 nodes, leading to 130 268 degrees of freedom (edges).

The potential projection pre-conditioning leads to lower CPU time to solve the matrix system. The repartition of the CPU time between the different phases of the E-fields calculation for the potential projection pre-conditioning is presented in figure 7.

Figure 8 shows the normalized SAR distribution in the yOz symmetry plane and figure 9 shows the normalized SAR distribution at 10 mm depth in the phantom in the half xOy plane. The normalized SAR is obtained by comparison with the maximum value of the SAR in the phantom.

$$\text{Normalized } SAR = \frac{SAR(\vec{r})}{\text{Maximum } SAR \text{ at } 10\,\text{mm depth}} \tag{21}$$

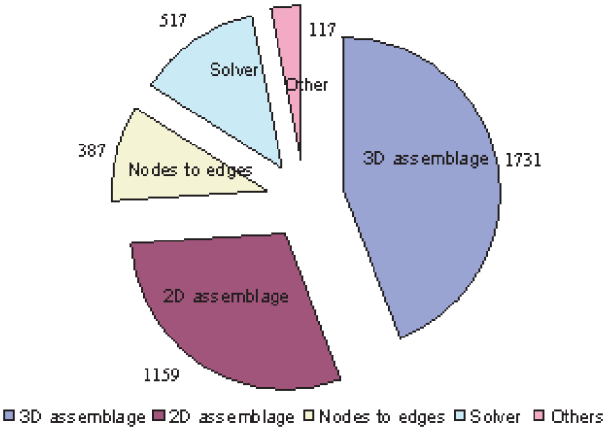

Figure 7. Repartition of CPU time (s) with the potential projection pre-conditioning.

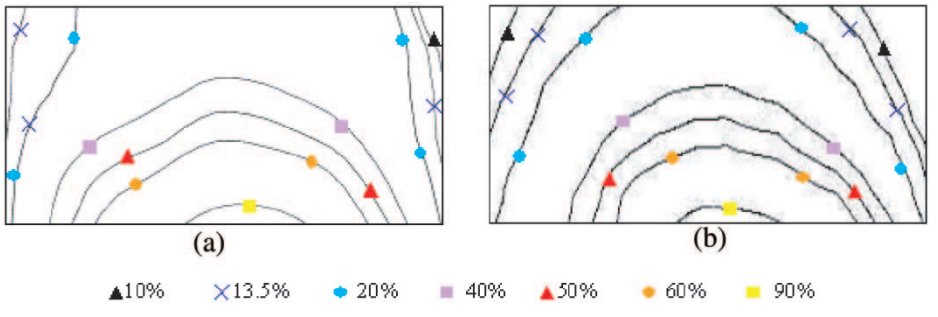

Figure 8. Comparison of calculated isoSAR distributions (*a*) on the yOz symmetry plane and temperature measurements (*b*) in muscle equivalent phantom.

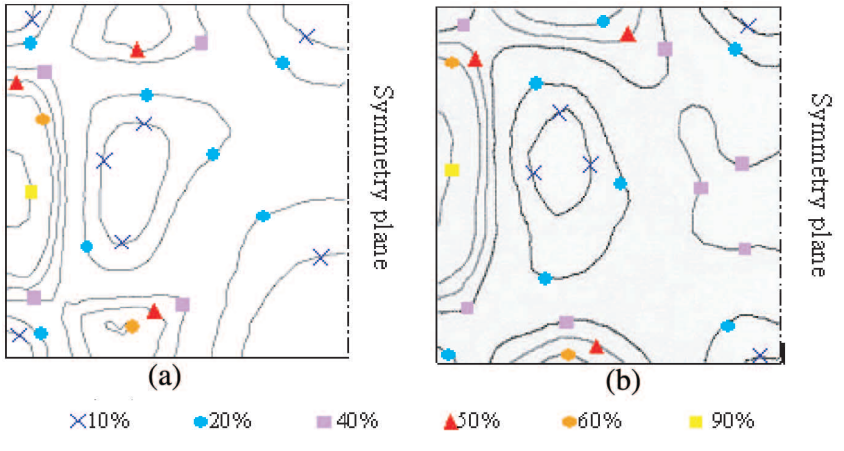

Figure 9. Temperature measurements at 10 mm depth on the xOy plane in muscle equivalent phantom (*b*) and corresponding numerical isoSAR distributions (*a*).

Comparison of predicted SAR and measured temperature shows a good global correlation. Slight differences may be explained by the presence of the 558 catheters (0.8 mm diameter) used for the temperature measurements. These catheters are filled with air and they are not modelled numerically. The experimental methodology, temperature measurement instead of field measurement, may also have some impact on the results.

In a second step, an interstitial hyperthermia treatment is modelled to show the ability of the model to handle several biological media and complex structures. Interstitial hyperthermia provides a viable alternative to other regional and local electromagnetic heating techniques and in many ways provides desirable heating characteristics[33]. Interstitial hyperthermia is very effective to heat deep-seated tumours, realizing an extremely localized temperature increase with a minimum risk of damage to surrounding healthy tissues[34]. In this study, the influence of the operating frequency of the antenna on the E-fields distribution is analysed (figure 10). The same geometry and mesh density for the inhomogeneous patient model are used, only the operating frequency of the antenna and the electromagnetic properties of these different media were modified (table 3). A transurethral interstitial applicator is used to increase the temperature in the bladder (figure 10(*a*)).

Comparison of the results for different frequencies (figure 10) shows that the E-field distribution for 915 MHz leads to the best focalization at the bladder level. The skin depth (δ) with interstitial applicators is only 60 mm (table 4), thus by this form of heat application the bladder would be heated sufficiently.

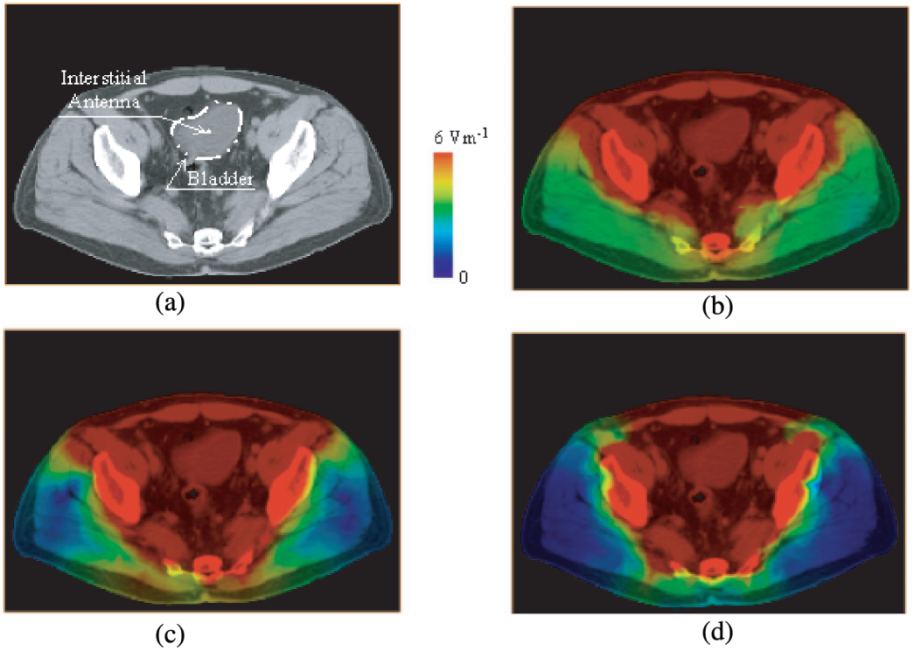

Figure 10. E-field distribution in a transverse section of the patient for different operating frequency of the interstitial antenna, 13.56 MHz (*b*), 433 MHz (*c*) and 915 MHZ (*d*).

Table 3. Properties (conductivity σ and permittivity ε_{real}) of biological tissues at the working frequencies 13.56, 433 and 915 MHz.

	13.56 MHz		433 MHz		915 MHz	
	ε_{real}	$\sigma\,(\mathrm{Sm}^{-1})$	ε_{real}	$\sigma\,(\mathrm{Sm}^{-1})$	ε_{real}	$\sigma\,(\mathrm{Sm}^{-1})$
Fat	11.83	0.030	5.567	0.042	5.46	0.051
Bone	30.57	0.045	13.07	0.095	12.44	0.145
Bladder	43.09	0.268	19.62	0.330	18.92	0.385
Muscle	138.44	0.628	56.87	0.805	55.00	0.948
Liver	181.27	0.336	50.69	0.668	46.76	0.861
Blood	210.64	1.12	63.84	1.36	61.31	1.544
Spleen	333.22	0.548	62.454	1.043	57.09	1.28
Intestine	362.75	1.386	65.29	1.92	59.39	2.17
Kidney	297.11	0.542	65.42	1.12	58.56	1.40

Table 4. Bladder properties (permittivity ε_{real}, conductivity σ, skin depth δ and wavelength λ) at the working frequencies 13.56, 433 and 915 MHz.

Frequency (MHz)	ε_{real}	$\sigma\,(\mathrm{Sm}^{-1})$	$\delta\,(\mathrm{m})$	$\lambda\,(\mathrm{m})$
13.56	43.09	0.268	0.280	1.56
433	19.62	0.330	0.075	0.148
915	18.92	0.385	0.061	0.074

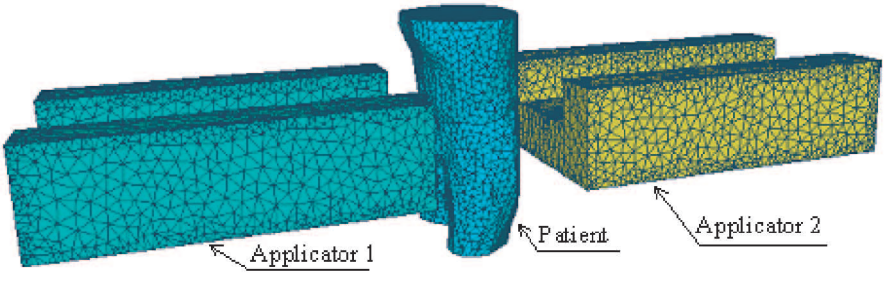

Figure 11. RF hyperthermia waveguides device and the patient model.

3.2. *Optimization of human patients: results and discussion*

To show the capabilities of the simulation and optimization tool, some computations based on a three-dimensional heterogeneous patient model have been performed. In these studies, the amplitude and phase of each antenna can be chosen separately. The capability of the optimization tool has been tested by considering two distinct hyperthermia devices: the waveguides configuration (figure 11) and the APA system (figure 12). The frequency of excitation is set to 27.12 MHz for the waveguides device and to 110 MHz for the APA system. The electrical characteristics of the biological tissues are presented in tables 5 and 6.

The optimal antenna parameters (amplitudes and phases) for the waveguides device are presented in table 7. The SAR distribution with the non-optimized and optimized parameters are shown in figure 13.

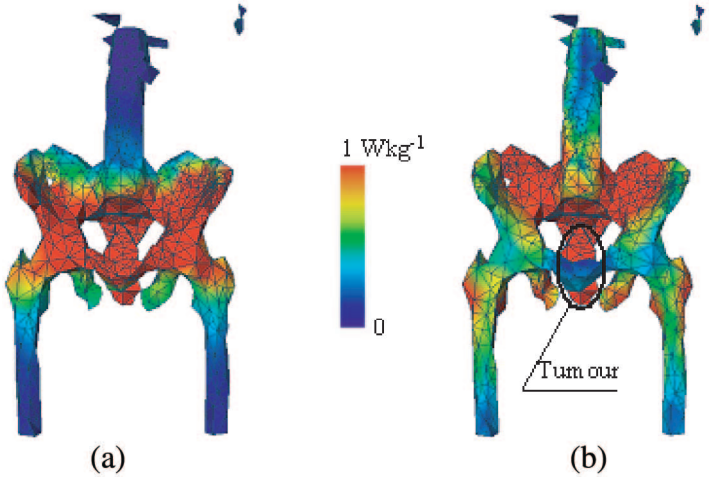

Figure 12. Patient model inside the annular phased array system.

Table 5. Properties of biological tissues at working frequency 27.12 MHz: permittivity ε, conductivity σ, skin depth δ, wavelength λ and density ρ.

	ε_{real}	ε_{imag}	σ (Sm^{-1})	δ (m)	λ (m)	ρ (kgm^{-3})
Air	1	0	0	—	11.06	—
Fat	8.4	21.90	0.033	0.642	2.772	900
Bone	21.8	33.18	0.05	0.588	1.995	1790
Bladder	31.46	185.84	0.28	0.199	1.055	1060
Tumour	60	530.97	0.8	0.114	0.642	1177
Muscle	95.8	431.42	0.65	0.134	0.675	1020
Liver	119.68	252.12	0.38	0.197	0.783	1050
Blood	126.6	769.91	1.16	0.097	0.519	1060
Spleen	188.24	424.78	0.64	0.150	0.612	1050
Intestine	202.49	982.30	1.48	0.088	0.451	1050
Kidney	187.9	411.50	0.62	0.153	0.618	1050

Table 6. Properties of biological tissues at working frequency 110 MHz: permittivity ε, conductivity σ, skin depth δ, wavelength λ and density ρ.

	ε_{real}	ε_{imag}	σ (Sm^{-1})	δ (m)	λ (m)	ρ (kgm^{-3})
Air	1	0	0	—	2.727	—
Fat	6	5.97	0.0365	0.391	1.014	900
Bone	15.05	10.64	0.065	0.334	0.667	1790
Bladder	22.3	48.27	0.295	0.110	0.444	1060
Tumour	60	130.91	0.8	0.067	0.270	1177
Muscle	64.95	116.51	0.712	0.074	0.274	1020
Liver	67.06	81.16	0.496	0.099	0.294	1050
Blood	75.3	202.91	1.24	0.052	0.226	1060
Spleen	87.44	133.2	0.814	0.072	0.245	1050
Intestine	93	273.27	1.67	0.044	0.197	1050
Kidney	94.62	135.16	0.826	0.073	0.239	1050

Table 7. Summary of optimization results.

Configurations	Applicator 1		Applicator 2		OF	$P_{patient}$ (W)	P_{tumour} (W)
	Ampl.	φ (°)	Ampl.	φ (°)			
Applicator 1	1	0	—	—	1.305	213	1.62
Applicator 2	—	—	1	0	1.746	133	1.22
Applicator 1 + 2 Default	1	0	1	0	1.522	484	4.31
Applicator 1 + 2 Optimized	1.304	0	2.991	235.46	2.297	1066	11.5

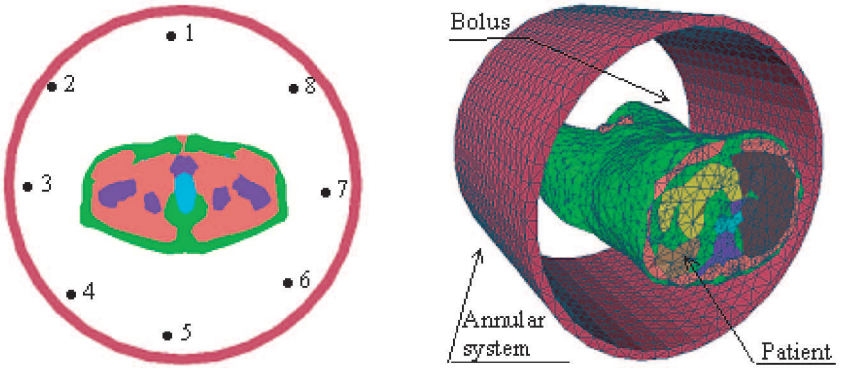

Figure 13. SAR distribution in the patient model. Left: manually adjusted parameters. Right: optimized antenna parameters. Note the increased heating of the tumour and the diminished hot spot near the frontal surface of the bone.

Table 8. Summary of optimization results.

Configurations	OF	$P_{patient}$ (W)	P_{tumour} (W)	SAR_{tumour} (Wkg^{-1})
Source 1	0.286	2.4	0.04	0.2
Four default sources (1, 3, 5, 7)	0.897	8.3	0.13	0.61
Four optimal sources (1, 3, 5, 7)	2.25	279.2	12.9	59.6
Eight default sources	1.18	53.7	0.82	3.50
Eight optimal sources	5.80	221	14.9	69.0

The second hyperthermia device is characterized by a dielectric ring and a set of eight antennae (figure 12). The working frequency is 110 MHz, which provides penetration and focalization compatible with clinical constraints.

The mesh of the first configuration is made of 42 089 nodes, 203 989 tetrahedral elements and 261 500 edges. For the APA system, the mesh contains 25 879 nodes, 146 364 tetrahedral elements leading to 174 937 degrees of freedom (edges).

Table 8 and figure 14 present the optimization results obtained with the GA method for the hyperthermia treatment with the APA device. Figure 14 represents the ratio between SAR in healthy tissues (fat, muscle, ...) and SAR in the tumour, this ratio must be as small as possible.

Table 9 presents the CPU time for the optimization procedure including the computation of the E-field for the eight antennae and the optimization process.

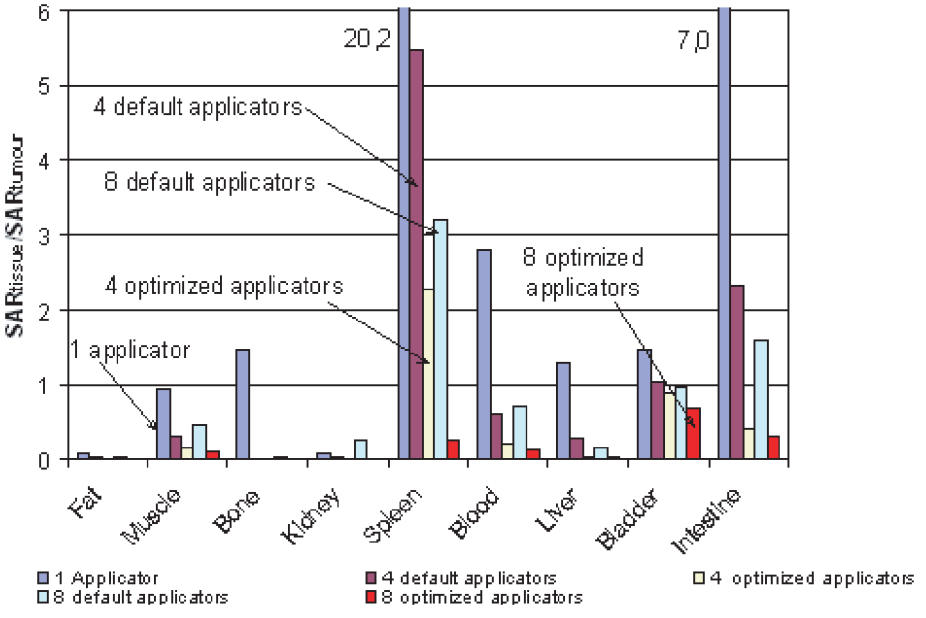

Figure 14. Ratio between the SAR in healthy tissues and the SAR in the tumour.

Table 9. CPU time of the optimization procedure (APA system).

		CPU time* (s)	
		Four sources	Eight sources
Electric field computation	Antenna 1	8 854	8 854
	Antenna 2		4 030
	Antenna 3	4 043	4 043
	Antenna 4		4 009
	Antenna 5	4 056	4 056
	Antenna 6		4 068
	Antenna 7	4 038	4 038
	Antenna 8		4 086
Optimization procedure (4 sources)		850	
Optimization procedure (8 sources)			1 208
Total		21 841	38 392

* On HP station J5000 PA risk processor with 1 Go of RAM.

The 3D assemblage and the passage nodes to edges are realized only for the first calculation (source 1) and stock, the next calculation for other sources used these stock values. The total CPU time for the global optimization procedure approaches 10 h for the configuration with eight sources.

4. Conclusion

The main aim of the presented work was to achieve localized hyperthermia in human tumour tissues by means of EM energy at RF or microwave frequency.

Accurate treatment planning will contribute greatly to optimal tumour temperature and to a successful hyperthermia treatment. An essential part of hyperthermia treatment planning is the SAR model. A formulation combining the FE method with GA optimization techniques has been developed to obtain the desired increased heat in the tumour region. Comparison of experimental and numerical data has demonstrated the ability of the FE model developed to predict the EM field distribution.

A procedure has been proposed for determining the excitation amplitudes and phases of the antennae of electromagnetic multi-applicator systems which yield an improved SAR distribution around deep-seated tumours. The proposed synthesis (FE and GA) has been demonstrated to provide a good focalization of the EM energy within the patient. The effectiveness of the method has been demonstrated through two studies with APA system and waveguides applicator device on realistic patient geometries obtained with CT scans. Besides, this method could be also extended to other kinds of applicators and other locations of the tumour. The hyperthermia treatment planning developed has provided much insight in the local hyperthermia treatment with electromagnetic applicators and allowed increasing the effective heating volume.

Further development of the optimization tool to optimize the delivery of energy and the temperature promise to significantly improve the ability of this technique to heat the tumour volume more uniformly. The next step of this work is oriented to the development of a numerical model to calculate the three-dimensional temperature distribution in tissues taking into account the blood circulation. The blood vessels such as arteries and veins will be modelled with discrete formalism and the small vessels (arterioles and venules) with continuous formalism. Three-dimensional models of SAR and temperature and the optimization procedure (GA) will be coupled to additional information about the actual temperature distribution within the patient with invasive thermometry and E-field sensors.

To summarize, the developed hyperthermia optimization tool has many fields of application. These include:

(a) The patient-specific optimization of settings, including positioning, phases and amplitudes.

(b) The evaluation of the clinical indications for a hyperthermia treatment. This assumes correct classification of easy to heat and difficult to heat tumours with hyperthermia treatment.

(c) The development of new antenna systems and applicators.

(d) The development of standard settings for some kind and location of tumours.

Acknowlegement

This paper was presented at the 21th annual meeting of ESHO Munich 2003.

References

1. Coley WB. The treatment of malignant tumors by repeated inoculations of erysipelas, with a report of ten original cases. *Am J Med Sci* 1893; 105: 487–511.
2. Van der Zee J, Gonzalez Gonzalez D. The dutch deep hyperthermia trial: results in cervical cancer. *Int J Hyperthermia* 2002; 18: 1–12.

3. Hildebrandt B, Wust P, Ahlers O, Dieing A, Sreenivasa G, Kerner T, Felix R, Riess H. The cellular and molecular basis of hyperthermia. *Crit Rev Oncol Hematol* 2002; 43: 33–56.
4. Ressel A, Schmitt O, Weiss C, Feyerabend T. Therapeutic outcome and side-effects after radiotherapy, chemotherapy and/or hyperthermia treatment of head and neck tumour xenographs. *Eur J Cancer* 2002; 38: 594–601.
5. Feyerabend T, Wiedemann GJ, Jäger B, Vesely H, Mahlmann B, Richter E. Local hyperthermia, and chemotherapy in recurrent breast cancer is feasible and effective except for inflammatory disease. *Int J Radiat Oncol Biol Phys* 2001; 49: 1317–25.
6. Lu B, Yang R, Lin W, Cheng KS, Wang C, Kuo T. Theoretical study of convergent ultrasound hyperthermia for treating bone tumors. *Med Eng Phys* 2000; 22: 253–63.
7. Lin W, Fan W, Yen J, Chen Y, Shieh M. A theoretical study of cylindrical ultrasound transducers for intracavitary hyperthermia. *Int J Radiat Oncol Biol Phys* 2000; 46: 1329–36.
8. Chou CK. Application of electromagnetic energy in cancer treatment. *IEEE Trans Instrument Meas* 1988; 37: 547–51.
9. Vrba J, Lapes M, Oppl L. Technical aspects of microwave thermotherapy. *Bioelectrochem Bioener* 1999; 48: 305–9.
10. James BJ, Sullivan DM. Creation of three-dimensional patient models for hyperthermia treatment planning. *IEEE Trans Biomed Eng* 1992; 39: 238–42.
11. Van der Zee J, Peer-Valstar JN, Rietveld PJM, Graaf-Strukowska L, Van Rhoon GC. Practical limitations of interstitial thermometry during deep hyperthermia. *Int J Radiat Oncol Biol Phys* 1998; 40: 1205–12.
12. Kroeze H, Van de Kamer JB, De Leeuw AAC, Kikuuchi M, Lagendijk JJW. Treatment planning for capacitive regional hyperthermia. *Int J Hyperthermia* 2003; 19: 58–73.
13. Kanai Y, Tsukamoto T, Saitoh Y, Miyakawa M, Kashiwa T. Analysis of a hyperthemic treatment using a reentrant resonant cavity applicator for a heterogeneous model with blood flow. *IEEE Trans Magnetics* 1997; 33: 2175–8.
14. Paulsen KD, Jia X, Sullivan JM. Finite element computations of specific absorption rates in anatomically conforming full-body models for hyperthermia treatment analysis. *IEEE Trans Biomed Eng* 1993; 40: 933–45.
15. Sabariego RV, Landesa L, Obelleiro F. Synthesis of an array antenna for hyperthermia applications. *IEEE Trans Magnetics* 2000; 36: 1696–9.
16. Webb JP. Edge elements and what they can do for you. *IEEE Trans Magnetics* 1993; 29: 1460–5.
17. Bossavit A. Edge elements for scattering problems. *IEEE Trans Magnetics* 1989; 25: 2816–21.
18. Engquist B, Majda A. Absorbing boundary conditions for the numerical simulation of waves. *Math Comp* 1977; 31: 629–51.
19. Perrussel R, Nicolas L, Mussy F. An efficient preconditioner for linear systems issued from the finite element method for scattering problems. *Proc 14th Conf Computation of Electromagnetic Fields COMPUMAG*, 13–18 July, Saratoga Springs, NY, USA, 2003; 14–15.
20. Boag A, Leviatan Y, Boag A. Analysis and optimization of waveguide multiapplicator hyperthermia systems. *IEEE Trans Biomed Eng* 1993; 40: 946–52.
21. Goldberg D. *Genetic Algorithms in search, optimization and machine learning*. Adisson Wesley, Don Mills, 1989.
22. Holland J. *Adaptation in natural and artificial systems*. Ann Arbor: University of Michigan Press, 1975.
23. Sareni B, Krahenbuhl L, Nicolas A. Niching genetic algorithms for optimization in electromagnetics, I. fundamentals. *IEEE Trans Magnetics* 1998; 34: 2984–7.
24. Wiersma J, Van Maarseveen RAM, Van Dijk JDP. A flexible optimization tool for hyperthermia treatments with RF phased array systems. *Int J Hyperthermia* 2002; 18: 73–85.
25. Wust P, Hiledebrandt B, Sreenivasa G, Rau B, Gellermann J, Riess H, Felix R, Schlag PM. Hyperthermia in combined treatment cancer. *Lancet Oncol* 2002; 3: 487–97.
26. Bini MG, Ignesti A, Millanta L. The polyacrylamide as a phantom material for electromagnetic hyperthermia studies. *IEEE Trans Biomed Eng* 1984; 31: 317–22.

27. Vera A. Contribution à l'étude d'un système d'hyperthermie profonde en cancérologie: automatisation du traitement du signal, modélisation, validation de la distribution et de l'absorption du champ électrique à 27.12 MHz dans les tissus simulés. Thesis. Dissertation, Institut National Polytechnique de Lorraine, Nancy, 1999.
28. Niederst C. Mise au point et intégration en clinique d'un programme prévisionnel de calcul de la répartition du champ électrique et des températures induites par des applicateurs électromagnétiques externes. Thesis. Dissertation, Université Paul Sabatier, Toulouse, 1997.
29. *Amira* [computer program]. Version 2.3. Indeed – Visual Concepts GmbH, Berlin, 1999.
30. Gabriel C, Gabriel S, Corthout E. The dielectric properties of biological tissues: I. Literature survey. *Phys Med Biol* 1996; 41: 2231–49.
31. Gabriel S, Lau RW, Gabriel C. The dielectric properties of biological tissues: II. Measurements in the frequency range 10 Hz to 20 GHz. *Phys Med Biol* 1996; 41: 2251–69.
32. Gabriel S, Lau RW, Gabriel C. The dielectric properties of biological tissues: III. Parametric models for the dielectric spectrum of tissues. *Phys Med Biol* 1996; 41: 2271–93.
33. Cherry PC, Iskander MF. FDTD analysis of power deposition patterns of an array of interstitial antennas for use in microwave hyperthermia. *IEEE Trans Microwave Theory Techn* 1992; 40: 1692–700.
34. Cerri G, De Leo R, Primiani VM. Thermic end-fire interstitial applicator for microwave hyperthermia. *IEEE Trans Microwave Theory Techn* 1993; 41: 1135–42.